# Electroweak radiative corrections to $\gamma\gamma \to W^+W^-$ in the two-Higgs-doublet model

Sun La-Zhen
*Joint Institute of ETH & USTC for High Energy Physics, Department of Modern Physics, University of Science and Technology of China, Hefei, Anhui, 230026, People's Republic of China*

Liu Yao-Yang
*Joint Institute of ETH & USTC for High Energy Physics, Department of Modern Physics, University of Science and Technology of China, Hefei, Anhui, 230026, People's Republic of China and Institute of Theoretical Physics, Academy of Sciences of China, Beijing 10080, People's Republic of China*

Zhang Ren-You
*Joint Institute of ETH & USTC for High Energy Physics, Department of Modern Physics, University of Science and Technology of China, Hefei, Anhui, 230026, People's Republic of China*

(Received 28 March 1997)

Electroweak radiative one-loop corrections to the process $\gamma\gamma \to W^+W^-$ with photon and W-boson polarizations are calculated within the two-Higgs-doublet model extension of the standard model, and the relevant analytical results for the nonstandard Higgs bosons contributions to the helicity amplitudes are given. The relative difference between the predictions of the two-Higgs-doublet model and minimal standard model for a light salar $M_{H_1}$ and heavy $M_{H_2}$ and $M_\Phi$ easily exceed $\pm 20\%$ for $W_TW_T$ pair production in the central angular region at high energy, and even larger for $W_LW_L$ pair production. The angular dependence corrections owing to the nonstandard Higgs boson get larger, where box diagrams constitute the dominant part of the radiative corrections. [S0556-2821(97)02621-0]

PACS number(s): 12.60.Cn; 12.15.Lk; 14.80.Cp

## I. INTRODUCTION

At present the successes of the standard model (SM) of electroweak interactions are well known and doubtless. In particular, measurements of the gauge boson masses $M_W$ and $M_Z$ and asymmetries of the $Z$ boson at the CERN $e^+e^-$ collider LEP have provided stringent constraints which are successfully predited by the SM evaluated at the one-loop level. However, the Higgs sector of the SM, consisting of a single Higgs doublet, has not yet been experimentally tested. Of course, before the physical Higgs boson $H_0$ is empirically detected, the Higgs mechanism cannot be conclusively confirmed. The Higgs boson mass $M_{H_0}$, which is a free parameter of the theory, enters all theoretical predictions within the SM at least via higher orders. In contrast with the top quark mass, the indirect limit on $M_{H_0}$ derived from radiative corrections to precision experiments is still rather weak but favor's a Higgs boson below 300 GeV. Experimentally, searching directly for the SM Higgs boson, the $e^+e^-$ collider LEP [1] has set a lower bound, $M_{H_0} > 64.5$ GeV (95% C.L.), on the Higgs boson mass, but does not exclude values up to $\sim 700$ GeV [2].

The possibility of an extended Higgs sector is definitely consistent with experimental data. The simplest extensions are models with the two-Higgs-doublet model (THDM) suggested by supersymmetry (SUSY) [3]; for such an extension, $\rho = 1$ remains automatic at the tree level. If $CP$ is conserved, then the THDM yields five physical Higgs $CP$ eigenstates: two $CP$-even neutral Higgs bosons $H_0$ and $H_1$, a $CP$-odd (pseudoscalar) Higgs boson $H_2$, a charged Higgs boson pair $\Phi^\pm$, and the mixing angles $\alpha$ and $\beta$, where $\alpha$ is the mixing angle of the $CP$-even Higgs bosons $H_0$ and $H_1$. An important parameter of the THDM is $\tan\beta = V_2/V_1$, where $V_2$ ($V_1$) is the vacuum expectation value of the neutral member of the Higgs doublet that couples to up-type (down-type) quarks. One neutral Higgs boson has a coupling similarly to the SM values.

Up to now, only weak direct experimental information has existed on the non-Abelian self-interaction of the gauge boson [4]. One can hope to obtain more information from $\gamma\gamma$ collisions because at high energies cross sections for $\gamma\gamma$ collisions are usually larger than those for $e^+e^-$ ones. High energetic photons are naturally generated via bremsstrahlung or beamsstrahlung in high energy $e^+e^-$ colliders. More efficiently an intense photon beam can be obtained by backward Compton-scattered laser light as already proposed by Ginzburg *et al.* [5]. The feasibility of such a photon linear collider is discussed in Ref. [6] based on the progress in collider and laser technology. The $\gamma WW$ and $\gamma\gamma WW$ couplings can be probed very effectively in the reaction $\gamma\gamma \to W^+W^-$ which does not involve the $ZWW$ coupling in lowest order. The sensitivity of the $\gamma\gamma \to W^+W^-$ cross section to various anomalous couplings has been discussed in Ref. [7] It offers information that is comparable to the that available from $e^+e^- \to W^+W^-$. The total cross section does not drop like $1/s$ as the one for $e^+e^- \to W^+W^-$ but approaches a constant of about 80 Pb at high energies. At the tree level the THDM may be identical to the SM. However, the THDM differs from the SM in that radiative corrections often depend rather sensitively on the details of the Higgs sector. Since in the non-SUSY two-Higgs-doublet model the masses and mixing angles can be considered as independent parameters, large or small radiative corrections can be ob-

 

tained to the process $\gamma\gamma\to W^+W^-$ and large deviations can occur from that in the SM by adjusting $\beta$ and other parameters.

Complete one-loop radiative corrections to $\gamma\gamma\to W^+W^-$ including soft photon bremsstrahlung in the context of the SM have been published in Ref. [8], so that in this paper we focus on the radiative corrections to the process $\gamma\gamma\to W^+W^-$ arising from the additional Higgs bosons within the THDM and give the complete analytical formula and extended discussion of the numerical results. The Feynman rules are taken from Ref. [3]. In order to evaluate a meaningful nonstandard correction, we adopt the conventional arrangement THDM that the mixing angles $\alpha=\beta$, where the neutral Higgs boson $H_0$ has the same couplings to $W^+W^-$ as the MSM Higgs boson, and $H_1, H_2, \Phi^{\pm}$ appear as additional nonstandard Higgs fields.

The paper is organized as follows: After fixing our notation and conventions in Sec. II, we briefly discuss the Born cross sections and the individual polarization possibilities in Sec. III. We give the analytical results for the radiative corrections classified by the topological structure of the corresponding Feynman diagrams in Sec. IV. A numerical evaluation and discussion of the radiative corrections for $\gamma\gamma\to W^+W^-$ follows in Sec. V. Finally Sec. VI contains a short summary.

## II. NOTATION AND CONVENTIONS

We consider the reaction

$$\gamma(k_1,\lambda_1)\,\gamma(k_2,\lambda_2)\to W^+(k_3,\lambda_3)W^-(k_4,\lambda_4), \qquad (1)$$

where $\lambda_{1,2}=\pm 1$ and $\lambda_{3,4}=0,\pm 1$ denote the helicities of the photon and the $W$ boson, respectively. The momenta read, in the center-of-mass system,

$$k_1^\mu=\frac{\sqrt{s}}{2}(1,0,0,-1), \quad k_2^\mu=\frac{\sqrt{s}}{2}(1,0,0,1),$$

$$k_3^\mu=\frac{\sqrt{s}}{2}(1,-\beta\ \sin\ \theta,0,-\beta\ \cos\theta),$$

$$k_4^\mu=\frac{\sqrt{s}}{2}(1,\beta\ \sin\theta,0,\beta\ \cos\theta), \qquad (2)$$

where $\beta=\sqrt{1-4M_W^2/s}$ is the velocity of the $W$ boson. Here $\theta$ is the scattering angle between the incoming photons and the outgoing $W$ boson. The Mandelstam variables read

$$s=(k_1+k_2)^2=(k_3+k_4)^2,$$

$$t=(k_1-k_3)^2=(k_2-k_4)^2=M_W^2-\frac{s}{2}(1-\beta\ \cos\theta),$$

$$u=(k_1-k_4)^2=(k_2-k_3)^2=M_W^2-\frac{s}{2}(1+\beta\ \cos\theta). \qquad (3)$$

In order to calulate the polarized cross section we introduce explicit polarzation vectors for the photon and $W$ boson as follows:

$$\varepsilon^{\mu_1}(k_1,\lambda_1=\pm 1)=-\frac{1}{\sqrt{2}}(0,1,\mp i,0),$$

$$\varepsilon^{\mu_2}(k_2,\lambda_2=\pm 1)=\frac{1}{\sqrt{2}}(0,1,\pm i,0),$$

$$\varepsilon^{*\mu_3}(k_3,\lambda_3=\pm 1)=-\frac{1}{\sqrt{2}}(0,\cos\theta,\pm i,-\sin\theta),$$

$$\varepsilon^{*\mu_4}(k_4,\lambda_4=\pm 1)=\frac{1}{\sqrt{2}}(0,\cos\theta,\mp i,-\sin\theta),$$

$$\varepsilon^{*\mu_3}(k_3,\lambda_3=0)=\frac{\sqrt{s}}{2M_W}(\beta,-\sin\theta,0,-\cos\theta),$$

$$\varepsilon^{*\mu_4}(k_4,\lambda_4=0)=\frac{\sqrt{s}}{2M_W}(\beta,\sin\theta,0,\cos\theta). \qquad (4)$$

Here $\lambda_i=\pm 1$ is the $\gamma$ or $W$ boson polarization vector with helicity $\pm 1$, and $\lambda_{3,4}=0$ is the longitudinal polarization vector of the $W$ boson. The electromagnetic gauge invariance tells us that the $\gamma\gamma\to W^+W^-$ polarization vector $G^{\mu_1,\mu_2,\mu_3,\mu_4}$ is transverse to the photon momenta:

$$k_1^{\mu_1}\varepsilon^{\mu_2}\varepsilon^{\mu_3}\varepsilon^{\mu_4}G_{\mu_1,\mu_2,\mu_3,\mu_4}=0$$
$$=k_2^{\mu_2}\varepsilon^{\mu_1}\varepsilon^{\mu_3}\varepsilon^{\mu_4}G_{\mu_1,\mu_2,\mu_3,\mu_4}. \qquad (5)$$

All momenta are taken to be on mass shell ($k_1^2=k_2^2=0$, $k_3^2=k_4^2=M_W^2$). The helicity amplitudes can be derived:

$$M_{\lambda_1,\lambda_2,\lambda_3,\lambda_4}=\varepsilon^{\mu_1}(\lambda_1)\varepsilon^{\mu_2}(\lambda_2)\varepsilon^{*\mu_3}(\lambda_3)\varepsilon^{*\mu_4}(\lambda_4)$$
$$\times G_{\mu_1,\mu_2,\mu_3,\mu_4}(k_1,k_2,k_3,k_4). \qquad (6)$$

The helicity amplitudes are the Bose and $CP$ parity symmetries

$$M_{\lambda_1,\lambda_2,\lambda_3,\lambda_4}(s,t,u,\beta)=M_{-\lambda_1,-\lambda_2,-\lambda_3,-\lambda_4}(s,t,u,\beta),$$

$$M_{\lambda_1,\lambda_2,\lambda_3,\lambda_4}(s,t,u,\beta)=M_{\lambda_2,\lambda_1,\lambda_4,\lambda_3}(s,t,u,\beta). \qquad (7)$$

In the following, we do not distinguish between the two transversly polarized $W$ bosons: then, we have the polarizations of the external pariticles by four labels, the first two corresponding to photons, and the second pair to $W$ bosons, $+$ for right handed, $-$ for left handed photons, $T$ for the sum of the two transverse polarizations, and $L$ for the longitude of $W$ polarizations.

## III. LOWEST ORDER CROSS SECTION

### A. Polarized cross sections for $WW$ pair production in monochromatic $\gamma\gamma$ collisions

We first present different contributions to the polarized cross sections for $WW$ pair production in monochromatic $\gamma\gamma$ collisions. We consider here the extreme cases of $\lambda_1\lambda_2 = \pm 1$, i.e., full circular polarization for incoming photons. The differential cross section is given by

$$\left(\frac{d\sigma_{\lambda_1,\lambda_2,\lambda_3,\lambda_4}(s)}{d\cos\theta}\right)^{\mathrm{THDM}} = \frac{\beta}{32\pi s}|M^{\mathrm{THDM}}_{\lambda_1,\lambda_2,\lambda_3,\lambda_4}|^2. \quad (8)$$

The tree level amplitudes agree in the MSM and the THDM, yielding (Fig. 1)

$$\begin{aligned} M_{\mathrm{Born}} = 4\pi\alpha\Bigg\{ & \frac{1}{M_W^2 - t}\{(\varepsilon_1\cdot\varepsilon_3)(\varepsilon_2\cdot\varepsilon_4)(k_1\cdot k_2 + 2k_1\cdot k_3 + k_3\cdot k_4) + (k_3 - k_4)\cdot\varepsilon_2[(\varepsilon_1\cdot\varepsilon_3)(k_1+k_3)\cdot\varepsilon_4 - 2(k_3\cdot\varepsilon_1) \\ & \times(\varepsilon_3\cdot\varepsilon_4) + (\varepsilon_1\cdot\varepsilon_4)(k_3 - 2k_1)\cdot\varepsilon_3] + (\varepsilon_2\cdot\varepsilon_4)[(k_3 - 2k_1)\cdot\varepsilon_3(k_4\cdot\varepsilon_1) - 2(k_3\cdot\varepsilon_1)(k_2+k_4)\cdot\varepsilon_3] \\ & + (k_1 - k_3 - k_2)\cdot\varepsilon_4[(k_3\cdot\varepsilon_4)(\varepsilon_1\cdot\varepsilon_3) - 2(k_3\cdot\varepsilon_1)(\varepsilon_2\cdot\varepsilon_3) + (\varepsilon_1\cdot\varepsilon_2)(k_3 - 2k_1)\cdot\varepsilon_3]\} - (\varepsilon_1\cdot\varepsilon_2)(\varepsilon_3\cdot\varepsilon_4) \\ & + (\varepsilon_1\cdot\varepsilon_3)(\varepsilon_2\cdot\varepsilon_4) + \text{``3''} \leftrightarrow \text{``4''}, t \to u\Bigg\}. \end{aligned} \quad (9)$$

The parameters $\alpha = 1/128$, $M_Z = 91.187$ GeV, $M_W = 80.33$ GeV, and $s_W^2 = 1 - M_W^2/M_Z^2$ have been used throughout the paper. In Fig. 2 we show the lowest order cross section in c.m. system (c.m.s.) energy for various polarizations, where the integrated cross sections are obtained from the angular range $10° \leqslant \theta \leqslant 170°$. The cross section of transverse $W_TW_T$ bosons increases with c.m.s. energy until reaches a plateau. At about 400 GeV it has almost reached this plateau and the total cross section is about 80 pb. The cross section for equal photon helicities and purely longitudinal $W$ bosons behaves like $1/s^3$ at high energies.

Figure 3 gives the angular distributions for $W_LW_L$, $W_LW_T$, and $W_TW_T$ pair production for equal and opposite incoming photon helicities at $\sqrt{s_{\gamma\gamma}} = 400$ GeV, 1 TeV, and 2 TeV. We see that the $W_TW_T$ and $W_LW_L$ pair production cross section is peaking in forward or backward directions for equal incoming photon helicities. The transverse $W$ pair production cross section will be at least an order of magnitude larger than the longitudinal $W$ pair production cross section.

### B. $WW$ pair production at a photon linear collider

The possiblity for the realization of $\gamma\gamma$ colliders has been discussed in detail by Ginzburg *et al.* [6]. The high degree of circular polarization for each of the colliding photons can be achieved by polarizing the incoming $e^-$ ($e^+$) beams and laser beams. The cross section for the $W^+W^-$ pair production in polarized $\gamma\gamma$ collisions can be obtained by folding the elementary cross section for the subprocesses $\gamma\gamma \to WW$ with the photon-photon luminosity ($dL_{\gamma\gamma}/d\tau$), i.e.,

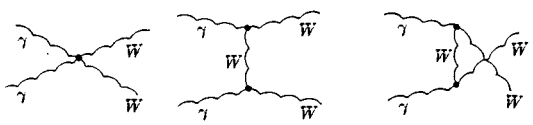


FIG. 1. Lowest order Feynman graphs for $\gamma\gamma \to W^+W^-$.

$$d\sigma_{\lambda_3\lambda_4} = \int_{4M_W^2/s}^{y_m^2} d\tau \frac{dL_{\gamma\gamma}}{d\tau}\left[\frac{1}{2}(1 + \langle\xi_1\xi_2\rangle)d\hat{\sigma}_{++\lambda_3\lambda_4} + \frac{1}{2}(1 - \langle\xi_1\xi_2\rangle)d\hat{\sigma}_{+-\lambda_3\lambda_4}\right], \quad (10)$$

where the photon-photon luminosity is

$$\frac{dL_{\gamma\gamma}}{d\tau} = \int_{\tau/y_m}^{y_m} \frac{dy}{y} f_\gamma(x,y) f_\gamma(x,\tau/y), \quad (11)$$

$$\tau = \hat{s}/s, \quad y = E_\gamma/E_b, \quad y_m = \frac{x}{1+x}, \quad x \equiv \frac{4E_b\omega_0}{m_e^2}.$$

Here $E_b$ is the energy of the electron beam and $\omega_0$ is the laser photon energy. The quantity $y$ stands for the ratio between the scattered photon and initial electron energies and its maximum value is $y_m$. The backscattered photon distribution function $f_\gamma(x,y)$ and mean helicities of the two photon beams $\xi_i$ are given by Eqs. (4) and (17) of Ref. [6]. Here

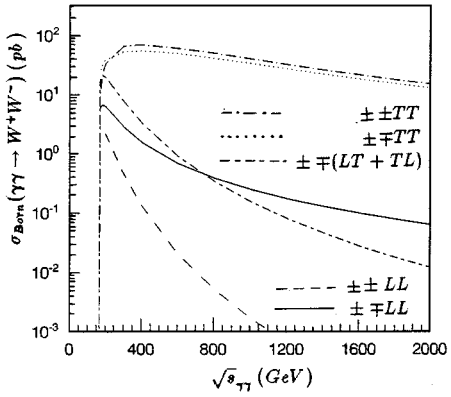


FIG. 2. Lowest order cross section versus c.m.s. energy for various polarizations ($10° < \theta < 170°$).

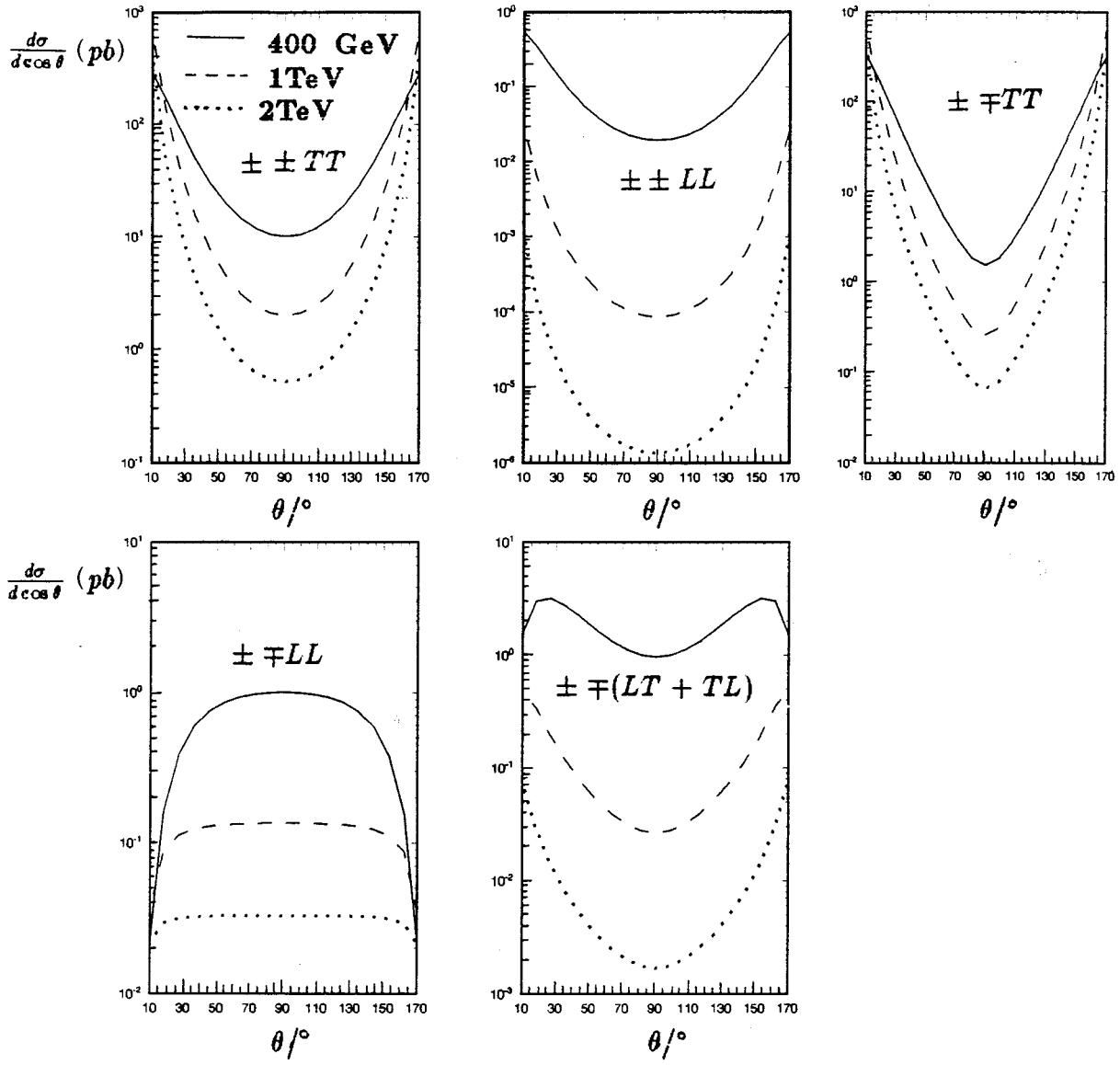


FIG. 3. Differential lowest order cross section versus c.m.s. energy photon helicities ($10°<\theta<170°$).

$\sqrt{s}$ ($\sqrt{\hat{s}}$) is the $e^+e^-$ ($\gamma\gamma$) center-of-mass energy. In the following we take the upper limit on $y_m$ to be 0.83, which leads to a good conversion efficiency in backward Compton scattering, and assume that 90% $e^-$ ($e^+$) beam longitudinal polarization ($\lambda_{e_{1,2}}=\pm 0.45$) and 100% laser beam circular polarization ($\lambda_{\gamma_{1,2}}=\pm 1$) are achievable.

In Fig. 4 we show the cross section of the $WW$ pair production at the photon linear collider as a function of the $e^-e^+$ c.m.s. energy with an angular cut $10°\leqslant\theta\leqslant 170°$. We consider different polarizations of the initial $e^-$ ($e^+$) and laser beams: $2\lambda_{e1,2}\lambda_{\gamma 1,2}=-0.9$, which gives the photon-photon energy spectrum peaking just below the highest allowed photon-photon energy. The relative polarizations $\lambda_{e1,2}$ and $\lambda_{\gamma 1,2}$ in Fig. 4 are such that colliding photons are produced mainly with equal (opposite) mean helicities, respectively. As for the case of monochromatic photon photon collisions, at high energies the cross section is dominated by transversely polarized $W_TW_T$ pair production. The advantage of having polarized beams is clearly seen. The cross section of longitudinal $W_LW_L$ pair production is the larger than that for the monochromatic photon spectrum at high energy, but at low energy the total cross section is the smaller than that.

## IV. ELECTROWEAK ONE-LOOP CORRECTIONS

The calculation of the radiative corrections is performed in the 't Hooft–Feynman gauge as worked out in Ref. [9]. The renormalization is carried through using the complete on-shell renormalization scheme. In this scheme all the fields are renormalized such that no external wave function renormalization is required; i.e., there are no self-energy corrections associated with external lines. For the process considered here, we only give the corrections to the $W$ propagator, to the $\gamma$ and $W$ vertices of the incoming photon and outgoing bosons, and box diagram contributions with additional Higgs bosons in the THDM. For a consistent treatment of the one-loop corrections the squared transition matrix element $|M|^2$ has to be expanded to a power series of the coupling constant to

$$|M|^{2\,\mathrm{THDM}}=|M_{\mathrm{Born}}|^2+2\,\mathrm{Re}|\delta M^{\mathrm{THDM}}M^{+}_{\mathrm{Born}}|+\text{higher order},$$

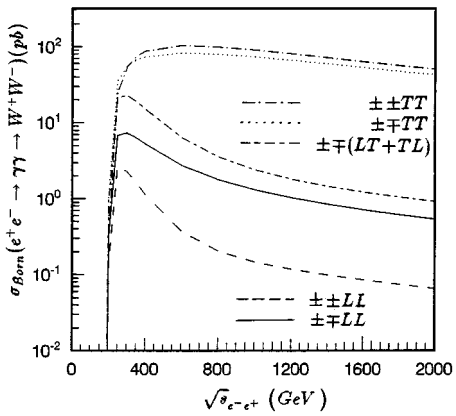


FIG. 4. The total $e^+e^- \to \gamma\gamma \to W^+W^-$ cross section for laser backcattered photons in $e^+e^-$ collisions as a function of the $\sqrt{s}_{e^+e^-}$. Curves for the combinations of the mean helicities of the incoming electron and laser beams $\lambda_{e1}=\lambda_{e2}=0.45$, $\lambda_{\gamma 1}=\lambda_{\lambda 2}=-1$, $\lambda_{e1}=-\lambda_{e2}=0.45$, and $\lambda_{\gamma 1}=-\lambda_{\lambda 2}=-1$ are shown.

where $\delta M^{\rm THDM}$ is the $O(\alpha)$ correction to the invariant matix element. The UV divergences are handled whthin dimensional regularization and the IR divergences are regularized by an infinitesimal photon mass $\lambda$. Adding soft photon bremsstrahlung the $\lambda$ dependence cancels out. The differential cross section, including the complete $O(\alpha)$ virtual and soft photonic corrections, is given by

$$\left(\frac{d\sigma}{d\cos\theta}\right)^{\rm THDM} = \frac{\beta}{32\pi s}[|M_{\rm Born}|^2(1+\delta_{\rm SB}) + 2\,{\rm Re}\{\delta M M^+_{\rm Born}\}] = \left(\frac{d\sigma}{d\cos\theta}\right)_{\rm Born}(1+\delta^{\rm THDM}) = \left(\frac{d\sigma}{d\cos\theta}\right)_{\rm Born}(1+\delta^{\rm MSM}+\delta^{\rm NS}), \quad (12)$$

where $\delta_{\rm SB}$ and $\delta^{\rm MSM}$ are the soft photon bremsstrahlung corrections and the relative electroweak corrections in the MSM, and $\delta^{\rm NS}$ is the relative weak corrections of nonstandard Higgs bosons in THDM. Since in this paper we are only interested in the nonstandard Higgs boson corrections in the THDM, we split all corrections into a MSM part and nonstandard (NS) part. $\delta_{\rm SB}$ and $\delta^{\rm MSM}$ corrections need not do be taken account. A detailed discussion of the MSM case is given in [8]. We now list the results for the nonstandard Higgs boson radiative corrections.

### A. Self-energies

Since external self-energies do not contribute in the complete on-shell renormalization scheme, only internal $W$ boson self-energy $\Sigma^{\rm NS}_{WW}(t,u)$ arising from the nonstandard Higgs bosons graphs in Fig. 5 yields the following contribution to $\delta M^{\rm NS}$:

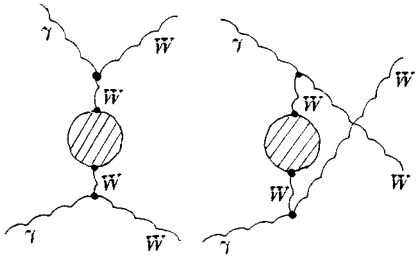


FIG. 5. Self-energy correction.

$$\delta M_{se} = -i4\pi\alpha\varepsilon_1\varepsilon_2\left\{ g_{\gamma WW^*}\frac{1}{t-M_W^2} \times\left(\frac{\Sigma^{\rm NS}_{WW}(t)-\delta M_W^{2\,{\rm NS}}}{t-M_W^2}+\delta Z_W^{\rm NS}\right) g_{\gamma W^*W} + g_{\gamma W^*W}\frac{1}{u-M_W^2} \times\left(\frac{\Sigma^{\rm NS}_{WW}(u)-\delta M_W^{2\,{\rm NS}}}{u-M_W^2}+\delta Z_W^{\rm NS}\right) g_{\gamma W^*W}\right\}\varepsilon_3\varepsilon_4. \quad (13)$$

The couplings between the photon and $W$ bosons ($\gamma W^*W$ vertex: asterisks denote off-shell fields) are denoted by $-ieg_{\gamma W^*W}$. The THDM renormalized constants and the conterterms expressed in terms of unrenormalized self-energies can be found in Ref. [10].

### B. Vertex corrections

The $t$-channel upper $\gamma W^*W$ vertex diagrams are depicted in Fig. 6, which are only those involving the nonstandard Higgs bosons. The diagrams for the lower $\gamma W^*W$ vertex can be constructed in an analogous way; the $u$-channel are obtained by interchange of the two external $W$ bosons. Extracting an overall factor $ie^2g^2/(4\pi)^2$, where $g=e/s_W$, in the definition of the helicity amplitudes $\delta M^{\rm ver}_{\lambda_1,\lambda_2,\lambda_3,\lambda_4}$, their analytical expressions are explicitly given in Appendix A.

The conterterm contribution to the matrix element is

$$\delta M_{\gamma W^*W} = -i4\pi\alpha\varepsilon_1\varepsilon_2 g_{\gamma W^*W}\left(\delta Z_e^{\rm NS}+\delta Z_W^{\rm NS}+\frac{1}{2}\delta Z_{AA}^{\rm NS} - \frac{c_W}{2s_W}\delta Z_{ZA}^{\rm NS}\right)\frac{1}{t-M_W^2}g_{\gamma W^*W}\varepsilon_3\varepsilon_4. \quad (14)$$

The photons are taken to be on mass shell, which do not mix

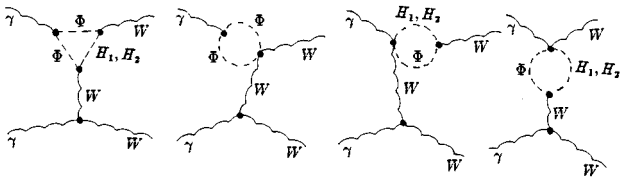


FIG. 6. The $t$-channel nonstandard Higgs boson diagrams for the upper $\gamma WW^*$ vertex.

FIG. 7. The $s$-channel nonstandard Higgs boson diagrams for the $\gamma\gamma H_0^*$ vertex in the THDM.

with $Z$ bosons, rendering the field renormalization constants $\delta Z_{ZA}^{\rm NS}$ zero.

The $s$-channel vertex corrections are the only Higgs pole contribution in Fig. 7. The $\gamma\gamma H_0^*$ vertex corrections only for equal initial photons or outgoing $W$ bosons helicities yield the contribution to $\delta M^{\rm NS}$:

$$\delta M^{\gamma\gamma H_0^*}_{++++} = (2M_{H_1}^2 + 4M_\Phi^2 - AM_{H_0}^2 \tan\beta) \times \frac{1}{s - M_{H_0}^2 + iM_{H_0}\Gamma_{H_0}} \left( \frac{B_0(k_1+k_2, M_\Phi, M_\Phi)}{2} - 2C_{24}(k_1, -k_3-k_4, M_\Phi, M_\Phi, M_\Phi) \right), \quad (15)$$

$$\delta M^{\gamma\gamma H_0^*}_{++00} = (2M_{H_1}^2 + 4M_\Phi^2 - AM_{H_0}^2 \tan\beta)(1+\beta^2) \times \frac{1}{4(s - M_{H_0}^2 + iM_{H_0}\Gamma_{H_0})} \left( \frac{B_0(k_1+k_2, M_\Phi, M_\Phi)}{2} - 2C_{24}(k_1, -k_3-k_4, M_\Phi, M_\Phi, M_\Phi) \right). \quad (16)$$

In this paper $A = \tan 2\alpha$. The definition of the two- and three-point functions $B$ and $C$ can be fond in Ref. [11].

### C. Box contributions

The nonstandard Higgs boson contributions in box diagrams are shown in Fig. 8. The corresponding analytical expressions denoted by the internal particles can be given in terms of the invariant functions $B$, $C$, and $D$ introduced in Ref. [11]. The explicit expressions for $\delta M^{\rm box}$ can be found in Appendix B.

The counterterm contribution to the matrix element is

$$\delta M_{\gamma\gamma WW} = -i4\pi\alpha\varepsilon_1\varepsilon_2 g_{\gamma\gamma WW} \times \left( -2\delta Z_e^{\rm NS} - \delta Z_W^{\rm NS} - \delta Z_{AA}^{\rm NS} + \frac{c_W}{2s_W}\delta Z_{ZA}^{\rm NS} \right) \varepsilon_3\varepsilon_4. \quad (17)$$

The complete one-loop virtual corrections are given by

$$\delta M^{\rm NS}_{\lambda_1,\lambda_2,\lambda_3,\lambda_4} = (\delta M_{se} + \delta M^{\rm ver}(t) + \delta M^{\rm ver}(u) + \delta M_{\gamma\gamma H*} + \delta M^{\rm box} + \delta M_{\gamma W*W}(t) + \delta M_{\gamma W*W}(u) + \delta M_{\gamma\gamma WW})_{\lambda_1,\lambda_2,\lambda_3,\lambda_4}. \quad (18)$$

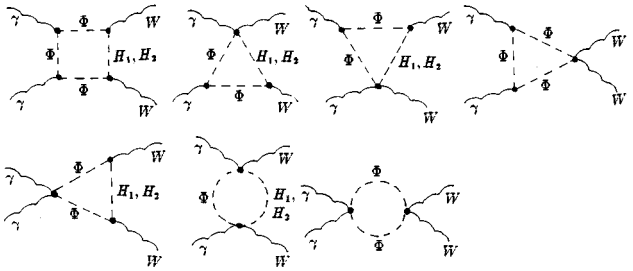

FIG. 8. Nonstandard Higgs boson box diagrams.

Various checks were carried out to make sure that the resulting helicity amplitudes are correct. The cancellation of divergences, the requirements of Bose symmetry, and gauge invariance (5) were explicitly checked. Morever, the formulas given in this section were produced by LIHIP [12]. A substantial part of these formulas was independently checked by hand calculation. The reduction of the tensor integrals to scalars was performed both numerically and computer algebraically with LIHIP, both programs agreeing to within 7 digits for each diagram separately.

## V. RESULTS AND DISCUSSION

The $O(\alpha)$ radiative corrections to the process $\gamma\gamma \to W^+W^-$ can be easily split in a gauge-invariant way into weak and electromagnetic corrections:

$$\delta = \delta_{\rm QED} + \delta_{\rm weak}.$$

The QED corrections are identical in the THDM and in the MSM and can be found in Ref. [8]. Furthermore, there are no new diagrams for the $W$ boson vertex and boxes. For the process considered here, we only give the weak corrections to the additional Higgs contributions in the THDM. Since we are interested in deviations of the THDM from the MSM, we introduce the quantites

$$\Delta(s)^{\rm NS} = \frac{\sigma^{\rm THDM}(s) - \sigma^{MSM}(s)}{\sigma_{\rm Born}(s)},$$

which directly give the nonstandard Higgs boson corrections. For the numerical evaluation, we use the same set of parameters as in Ref. [13]. For the Higgs sector of the THDM we choose $\alpha_{\rm em}$, $M_Z$, $M_W$, $M_{H_0}$, $M_{H_1}$, $M_{H_2}$, $M_\Phi$, and $\beta$ as input paramerters and set $\alpha = \beta$. This has the advantage that the particles of the MSM and their couplings form a subset of the THDM identical to $H_0$, the MSM Higgs boson. Here we will present the numerical results for a monochromatic photon beam with 100% circular polarization; such an idealized case will provide a clear physical understanding of the behavior of the cross sections.

The difference beween the THDM and MSM, i.e., the nonstandard corrections $\Delta^{\rm NS}(s)$ shown for the process $\gamma\gamma \to W^+W^-$ in Fig. 9 for different boson polarizations with $M_{H_1} = 50$ GeV, $M_{H_2} = 100$ GeV, $M_{H_0} = 200$ GeV, $M_\Phi = 400$ GeV, and $\tan\beta = 50$, is large. As already pointed out in Ref. [8], for the corrections to $W_L W_L$, there is a large positive correction enhanced. This effect originates from the sup-

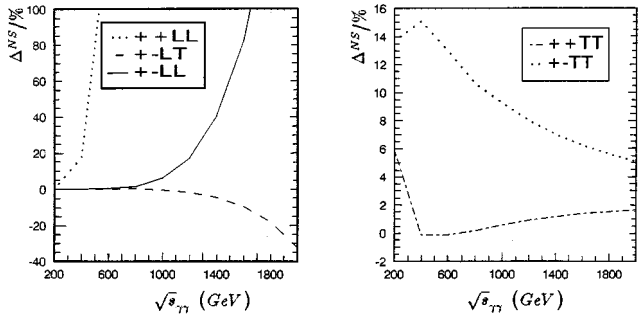


FIG. 9. Relative corrections $\Delta^{\mathrm{NS}}$ for several polarizations with $M_{H_1}=50$ GeV, $M_{H_2}=100$ GeV, $M_{\Phi}=400$ GeV, and $M_{H_0}=200$ GeV.

pression of the corresponding lowest order cross section and is proportional to $M_H^2/M_W^2$ which increases very fast with increasing energy. It amounts to more than three orders of magnitude at 2 TeV. While the corrections for opposite photon polarizations and mixied transverse and longitudinal $W$ boson polarizations are suppressed by an additional factor $1/s$ at high energy and reach $-30\%$ at $\sqrt{s}_{\gamma\gamma}=2$ TeV, the transverse $W_TW_T$ bosons get corrections of 5%. The corrections for the MSM are typically of the order of 10%. One gets large differences between THDM and MSM results owing to the enhancement of the box correction. The lowest order contribution for $\gamma\gamma \to W^+W^-$ exhibits a $t$ or $u$ pole but is not of order $1/s$ for all scattering angles. Thus the relative box corrections are large because of the smallness of the lowest order cross section for central angular region. In Fig. 10 we show the nonstandard Higgs boson contribution corrections to the differential cross sections for $\sqrt{s}_{\gamma\gamma}=0.4$, 1, and 2 TeV. The anguar distribution for longitudinal $W$ bosons is rather large at 90° scattering angle and depends more strongly on the energy, which is suppressed by the lowest order cross section. The corrections for transverse $W$ bosons are small in the forward and backward directions owing to the suppression of the $t$- and $u$-channel poles in lowest order and reach $-30\%$ (10%) for equal (opposite) helicity photons at intermediate scattering angles.

The Higgs boson resonances via $\gamma\gamma \to H_0^* \to W^+W^-$, this vertex exists only at the one-loop level, have been calculated in the MSM of Ref. [14]. This process is well suited

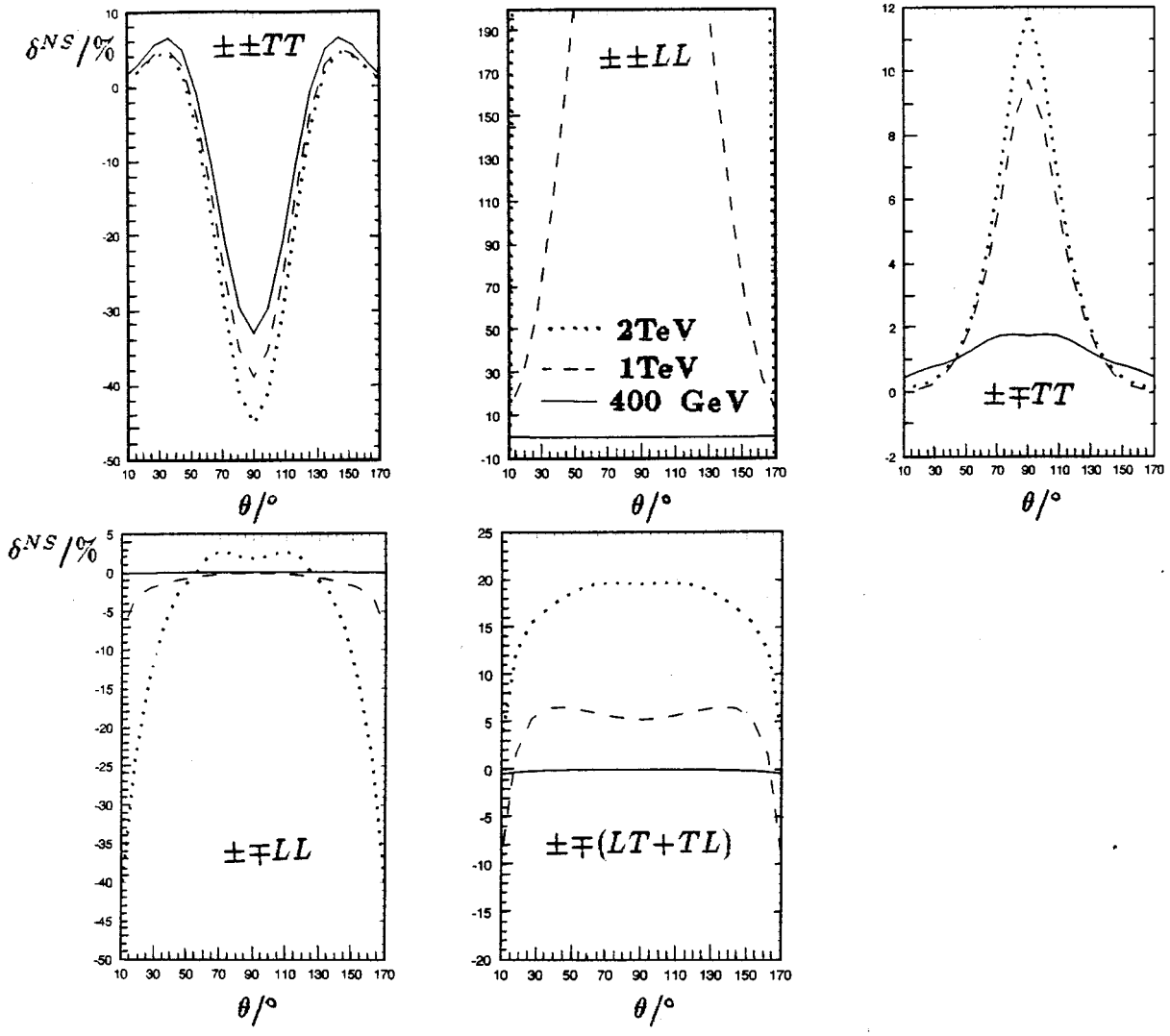


FIG. 10. The angular dependence of the $\delta^{\mathrm{NS}}$ (same signature as in Fig. 9).

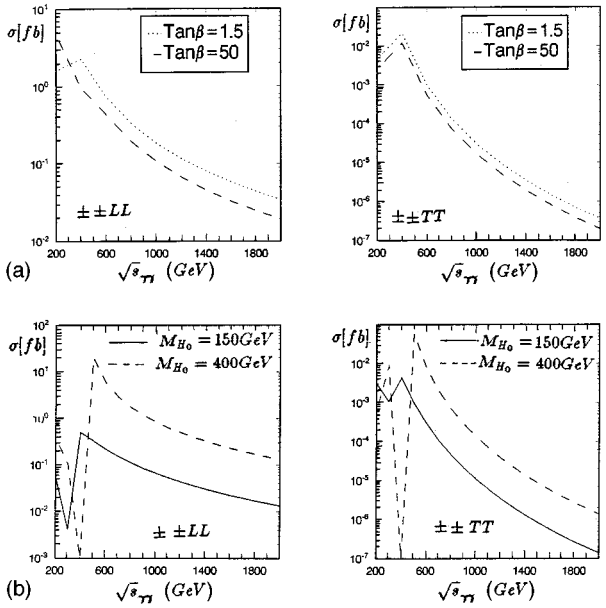


FIG. 11. The nonstandard part of the resonant cross section $\gamma\gamma\to H^*\to W^+W^-$: (a) $M_{H_1}=50$ GeV, $M_{H_2}=M_\Phi=200$ GeV, $M_{H_0}=250$ GeV, and tan$\beta$=1.5 and 50. (b) $M_{H_1}=50$ GeV, $M_{H_2}=M_\Phi=200$ GeV tan$\beta$=1.5, and $M_{H_0}=150$ and 400 GeV.

for Higgs boson studies at $\gamma\gamma$ colliders if $M_H>2M_W$. The nonstandard Higgs contribution Higgs resonant part of the process is given in Fig. 11. The helicity conservation of the cross sections is nonzero only for equal photon and $W$ boson helicities. We give the cross section of the $W_TW_T, W_LW_L$ production with $M_{H_1}=50$ GeV, $M_{H_2}=M_\Phi=200$ GeV, and $M_{H_0}=250$ GeV for tan$\beta$=1.5 and 50, and take the condition $\alpha=\beta$ in Fig. 11(a). As can be seen the sensitivity to the cross section is weak for tan$\beta\gg1$. For equal initial photon helicities, the value of the cross section of $W_LW_L$ pair production is about 2 fb or less [Fig. 11(b)], which is larger than for ones of transversely polarized $W_TW_T$ pair production.

## VI. SUMMARY

The process $\gamma\gamma\to W^+W^-$ is very useful to study the nonabelian gauge coupling $\gamma WW$ and $\gamma\gamma WW$. We have calculated the one-loop nonstandard Higgs boson corrections corresponding to $\gamma\gamma\to W^+W^-$ within the THDM. The relevant analytical formulas for polarized photons and $W$ bosons have been given. The calculation shows that the dominating corrections aries not only from the self-energies and renormalization constants but notable also from the box diagrams. At high energies and in the forward and backward directions, the corrections for transverse $W$ bosons are smaller owing to the suppression of the lowest-order $t$- and $u$-channel poles. The contribution involving the $1/t$ pole together with the smallness of the lowest order cross section leads to extremely large corrections at high energies for longitudinal $W$ polarizations.

## ACKNOWLEDGMENTS

This work was supported in part by the National Education Committee Foundation of China under Grant No. 9435809 and the National Natural Science Foundation of China.

## APPENDIX A: VERTEX CORRECTIONS

The nonstandard Higgs sector contributions to the $t$-channel upper $\gamma W^*W$ vertex corrections given by the explicit expressions for the functions $C_{ij}$ are given in Ref. [11].

$$\delta M^{\rm ver}_{++++}=\frac{1}{(\beta\cos\theta-1)}\left\{\frac{(1+\cos\theta)^2}{4s}[2M_W^2C'_{24}+(2s+M_W^2-u)C'_{35}-2(s-M_W^2-u)C'_{36}]+\frac{\beta(1+\cos\theta)\sin^2\theta}{16}\right.$$
$$\times[2M_W^2C'_{12}-2s(s-M_W^2-u)C'_{22}+(s+4M_W^2-u)C'_{23}+(2s+M_W^2-u)C'_{33}-2(s-M_W^2-u)C'_{34}]$$
$$-\sin\theta(C'_{24}+C'_{35})+\frac{\beta\sin^2\theta}{4}[(\cos\theta-3)(C'_{24}+C'_{36})+(3\cos\theta-1)C'_{35}]+\frac{\beta^2\sin^2\theta}{4}(\cos\theta+19)C'_{36}$$
$$\left.+\frac{\beta^2s\sin^4\theta}{8}(C'_{23}+C'_{33}-C'_{22}-C'_{34})\right\},\tag{A1}$$

$$\delta M^{\rm ver}_{+++-}=\frac{\sin^2\theta}{(\beta\cos\theta-1)}\left\{\frac{(\cos^2\theta-1)}{2s\sin^2\theta}[M_W^2C'_{24}+(s+M_W^2-u)C'_{35}-(s-M_W^2-u)C'_{36}]+\frac{\beta(\cos\theta-1)}{8}\right.$$
$$\times[M_W^2C'_{12}-(s-M_W^2-u)C'_{22}+(s+2M_W^2-u)C'_{23}+(s+M_W^2-u)C'_{33}-2(s-M_W^2-u)C'_{34}+2C'_{36}]-(C'_{24}+C'_{35})$$
$$\left.+\frac{\beta}{4}[(3+\cos\theta)C'_{24}+(5+3\cos\theta)C'_{35}]-\frac{\beta^2s\sin^2\theta}{8}(C'_{22}-C'_{23}-C'_{33}-C'_{34})\right\},\tag{A2}$$

$$\delta M^{\rm ver}_{++00}=\frac{\sin^2\theta}{(\beta\,\cos\theta-1)}\Bigg\{[s(\beta^2-\cos^2\theta)-2\beta s(\beta-\cos\theta)(\beta-\cos\theta+1)]\,\frac{(C'_{24}+C'_{35})}{4\sin^2\theta}-\frac{\beta^2 s(\beta+\cos\theta)}{4\sin^2\theta}C'_{36}$$
$$+\frac{\beta s(\beta-\cos\theta)}{32}[s(C'_{12}+3C'_{23}+2C'_{33})-(s-2M_W^2)(C'_{12}+2C'_{22}-C'_{33}-2C'_{34})-2(M_W^2-u)$$
$$\times(C'_{22}-C'_{23}+C'_{33}-C'_{34})]+\frac{[2M_W^2+\beta s(\beta-\cos\theta)]}{8}C'_{24}+\frac{(s+M_W^2-u)}{4}C'_{35}-\frac{\beta s(\beta+2\cos\theta)}{8}C'_{35}$$
$$+\frac{\beta^2 s(3+\beta^2)}{4}C'_{36}-\frac{2(s-M_W^2-u)+\beta s(\beta+2\cos\theta)]}{8}C'_{36}\Bigg\}, \tag{A3}$$

$$\delta M^{\rm ver}_{+-++}=\frac{\sin^2\theta}{(\beta\,\cos\theta-1)}\Bigg\{\frac{(\cos^2\theta-1)}{2s\,\sin^2\theta}[M_W^2C'_{24}+(3M_W^2-u)C'_{35}-(s-M_W^2-u)C'_{36}]+\frac{\beta(\cos\theta-1)}{8}$$
$$\times[M_W^2C'_{12}-(s-M_W^2-u)C'_{22}+(s+2M_W^2-u)C'_{23}-(s-M_W^2-u)C'_{34}+2C'_{24}]-\frac{1}{4}(C'_{24}+4C'_{35})$$
$$+\frac{\beta}{4}[(3\cos\theta+1)C'_{35}+\beta(17+\cos\theta)C'_{36}-(5+3\cos\theta)C'_{36}]+\frac{\beta^2 s\,\sin^2\theta}{16}(C'_{23}-C'_{22}+C'_{33}+C'_{34})\Bigg\}, \tag{A4}$$

$$\delta M^{\rm ver}_{+-+-}=\frac{\sin^2\theta}{(\beta\,\cos\theta-1)}\Bigg\{\frac{(\cos^2\theta+1)^2}{2s\,\sin^2\theta}[M_W^2C'_{24}+(s+M_W^2-u)C'_{35}-(s-M_W^2+u)C'_{36}]^+\,\frac{\beta(1+\cos\theta)}{8}$$
$$\times[M_W^2C'_{12}-(s-M_W^2+u)C'_{22}+(s+2M_W^2-u)C'_{23}+(s+M_W^2-u)C'_{33}-2(s-M_W^2-u)C'_{34}]$$
$$+\frac{\beta}{4}[2\cos\theta C'_{24}+(5+3\cos\theta)C'_{35}]+\frac{\beta(1+\cos\theta)}{4}C'_{36}+\frac{\beta^2 s\,\sin^2\theta}{8}(C'_{23}+C'_{33}-C'_{22}-C'_{34})\Bigg\}, \tag{A5}$$

$$\delta M^{\rm ver}_{+-+0}=\frac{\sin\theta\sqrt{s}}{(\beta\,\cos\theta-1)\sqrt{2}M_W}\Bigg\{\frac{(\cos\theta+1)}{4}\Bigg[\left(\beta^2-\cos\theta+\frac{2M_W^2}{s}\right)C'_{24}+2\left[1+\frac{M_W^2-u}{s}-\beta(\beta+\cos\theta)\right]C'_{35}$$
$$+2\left(2\beta\,\cos\theta-\frac{(s-M_W^2-u)}{s}\right)C'_{36}\Bigg]+\sin^2\theta\Bigg[\frac{\beta}{8}[M_W^2C'_{12}-(s-M_W^2-u)C'_{22}+(s+2M_W^2-u)C'_{23}$$
$$+(s+M_W^2-u)C'_{33}-(s-M_W^2-u)C'_{34}+\cos\theta C'_{24}+2(C'_{35}+C'_{36})]+\frac{\beta^2 s(\cos\theta-\beta)}{16}(C'_{12}+2C'_{22}+C'_{23}+2C'_{34})\Bigg]\Bigg\} \tag{A6}$$

$$\delta M^{\rm ver}_{+-00}=\frac{\beta s\,\sin^2\theta}{(\beta\,\cos\theta-1)M_W^2}\Bigg\{\frac{(\beta-\cos\theta)}{32}[(2M_W^2-\beta s\,\cos\theta)C'_{12}-[s(1-2\beta^2)-4M_W^2+u]C'_{22}$$
$$-[\beta s(2\beta+3\cos\theta)+u-2s-3M_W^2]C'_{23}+2[s+M_W^2-u-\beta s(\beta+\cos\theta)]C'_{33}+2[s(\beta^2-1)+M_W^2+u]C'_{34}]$$
$$+\left(2\beta-\cos\theta+\frac{4M_W^2}{\beta s}\right)\frac{C'_{24}}{16}+\frac{1}{4\beta s}[(s+M_W^2-u)C'_{35}-(s-2M_W^2+u)C'_{36}]$$
$$-\frac{1}{8}[(\beta+3\cos\theta)C'_{35}-(\beta-3\cos\theta)C'_{36}-2\beta(2+\beta^2)C'_{36}]\Bigg\}, \tag{A7}$$

with

$$C'_{i,j}=C_{i,j}(k_1,-k_3,M_\Phi,M_\Phi,M_{H_1})+C_{i,j}(k_1,-k_3,M_\Phi,M_\Phi,M_{H_2}).$$

We do not consider those polarization configurations for which the lowest order matrix element vanishes.

## APPENDIX B: BOX CORRECTIONS

The nonstandard Higgs bosons contribution box corrections to $\gamma\gamma\to W^+W^-$ matrix element are given, for which only nonzero terms after the interference with the Born matrix element will be given explicitly:

$$\delta M^{\rm box}_{++++}=\beta s\ \sin^2\theta\Big\{\frac{\beta}{4}[(\cos\theta+29)D'_{420}-16D'_{416}]-\frac{1}{2\beta}(D'_{417}+D'_{418}-2D'_{421})$$
$$-\frac{1}{2}[D'_{418}+2\cos\theta(D'_{419}-D'_{420})-(\cos\theta-1)D'_{421}]+\frac{\beta s\ \sin\theta}{16}(2D'_{413}-D'_{410}-D'_{411})$$
$$+\frac{1+\cos\theta}{16}(2C^1_{23}-2C^1_{22}+C^2_{22}-C^2_{23})\Big\}-[4+2(\cos^2\theta+1)]D'_{422}-\frac{(1+\cos\theta)^2}{4}(2C^1_{24}-C^2_{24})$$
$$+\frac{(1+\cos\theta)^2}{16}B^1_0-8C^3_{24}+4C^4_{24}+B^2_0, \tag{B1}$$

$$\delta M^{\rm box}_{++00}=\frac{s}{M_W^2}\Big\{\frac{s}{4}(\beta^2-\cos^2\theta)(D'_{417}+D'_{418})-\frac{1}{2}\beta s(\beta-\cos\theta)D'_{419}-\frac{s}{2}\beta(\beta+\cos\theta)D'_{420}+\frac{s}{2}(\beta^2+\cos^2\theta)D'_{421}-s(1$$
$$+\beta^2)D'_{422}-s\ \sin^2\theta D'_{422}+\beta s\ \sin^2\theta\Big(\frac{\beta s}{32}(9\beta^2-\cos^2\theta)D'_{410}+(\beta^2-\cos^2\theta)D'_{411}+2(\beta^2+\cos^2\theta)D'_{413}$$
$$-\frac{\beta}{8}[(5+\beta^2)D'_{416}+4D'_{418}-2D'_{420}]+\frac{\cos\theta}{2}(D'_{419}-D'_{420})+\frac{\beta^3 s}{16}(4D'_{43}-D'_{45}-8D'_{48})$$
$$-\frac{\beta^2 s}{16}[(\beta-\cos\theta)D'_{44}-\cos\theta D'_{45}]\Big)+\frac{\beta s(\beta-\cos\theta)\sin^2\theta}{32}(2C^1_{22}-2C^1_{23}+C^2_{22}-C^2_{23})$$
$$+\frac{\sin^2\theta}{32}(4C^2_{24}-8C^1_{24}+B^1_0)+\frac{(1+\beta^2)}{4}(B^2_0+4C^4_{24}-8C^3_{24})-\frac{\beta^2 s}{2}(C^4_{22}+C^4_{23})\Big\}, \tag{B2}$$

$$\delta M^{\rm box}_{+++-}=-2(\cos^2\theta-1)D'_{422}-\frac{s\ \sin^2\theta}{2}(D'_{417}+D'_{418}-D'_{421})-\frac{\beta s\ \sin^2\theta}{2}\Big[(\cos\theta-1)(D'_{418}-D'_{421})+2\cos\theta(D'_{419}-D'_{420})$$
$$-\frac{\beta s\ \sin^2\theta}{8}(D'_{410}+D'_{411}-2D'_{413})+\frac{(1+\cos\theta)}{4}(C^1_{23}-C^1_{22})+\frac{(\cos\theta-1)}{16}(C^2_{22}-C^2_{23})\Big]$$
$$+\frac{(\cos^2\theta-1)}{4}\Big(C^2_{24}-2C^1_{24}+\frac{1}{4}B^1_0\Big), \tag{B3}$$

$$\delta M^{\rm box}_{+-++}=\frac{\beta s\ \sin^2\theta}{4}\{\beta[(27+\cos\theta)D'_{420}-16D'_{416}-14D'_{418}]+4\cos\theta(D'_{420}-D'_{419})-[2\cos\theta+\beta(\cos\theta-1)]D'_{418}\}$$
$$+\frac{s\ \sin^2\theta}{2}[(2+\cos\theta)D'_{421}-D'_{417}-D'_{418}]+\frac{\beta^2 s^2\ \sin^4\theta}{16}(2D'_{413}-D'_{410}-D'_{411})+\frac{\cos^2\theta-1}{16}(4C^2_{24}-8C^1_{24}+B^1_0)$$
$$+\frac{\beta s\ \sin^2\theta}{16}[(1+\cos\theta)(C^1_{23}-C^1_{22})+(\cos\theta-1)(C^2_{22}-C^2_{23})], \tag{B4}$$

$$\delta M^{\rm box}_{+-+-}=\frac{\beta s\ \sin^2\theta(1+\cos\theta)}{16}(16D'_{420}-16D'_{419}+2C^1_{23}-2C^1_{22}+C^2_{22}-C^2_{23})+\frac{\beta s\ \sin^2\theta}{2}(D'_{421}-D'_{418})$$
$$+\frac{\beta^2 s^2\ \sin^4\theta}{16}(2D'_{412}+2D'_{413}+2D'_{43}-4D'_{49}-D'_{410}-D'_{411})+\frac{(1+\cos\theta)^2}{16}(4C^2_{24}-8C^1_{24}+32D'_{422}+B^1_0), \tag{B5}$$

$$\delta M^{\rm box}_{+-+0}=\frac{\sqrt{s}\,\sin\theta}{\sqrt{2}M_W}\Big\{-(1+\cos\theta)(\beta s D'_{416}+2D'_{422})+\frac{\beta^2 s}{2}(1+\cos\theta)(3D'_{420}-D'_{418})+\frac{\beta s}{2}(1+\cos\theta)(\beta+\cos\theta)$$
$$\times(D'_{419}-D'_{420})+\frac{\beta^2 s^2\,\sin^2\theta}{16}(\beta+\cos\theta)(D'_{410}+2D'_{412}-4D'_{414})+\frac{\beta s^2\,\sin^2\theta}{16}[(\cos\theta-9\beta)D'_{411}$$
$$+2(2\beta-\cos\theta)D'_{413}+4(2\cos\theta-\beta)D'_{415}+2(\cos\theta-\beta)D'_{43}$$
$$+4(2\beta-\cos\theta)D'_{48}-4\cos\theta D'_{49}]-\frac{\beta s\,\sin^2\theta}{2}(D'_{419}+D'_{420})+\frac{\beta^3 s^2\,\sin^2\theta}{8}(D'_{45}-D'_{44})+\frac{\beta s}{8}(\beta-\cos\theta)$$
$$\times(1+\cos\theta)(C^1_{23}-C^1_{22})+\frac{\beta s\,\sin^2\theta}{16}(C^2_{22}-C^2_{23})+\frac{1+\cos\theta}{16}(4C^2_{24}-8C^1_{24}+B^1_0)\Big\}, \tag{B6}$$

$$\delta M^{\rm box}_{+-00}=\frac{s\,\sin^2\theta}{16M_W^2}\Big\{\frac{\beta^2 s^2}{2}[(\beta^2-\cos^2\theta)D'_{410}+(9\beta^2-\cos^2\theta)D'_{411}+(\beta^2+\cos^2\theta)D'_{413}]$$
$$-\beta^2 s[(5+\beta^2)D'_{416}+4D'_{418}-4D'_{420}]+8\beta s\,\cos\theta(D'_{419}-D'_{420})-\beta^3 s^2(D'_{44}-\cos\theta D'_{45})$$
$$+\beta^4 s^2(4D'_{43}-D'_{45}-8D'_{48})+\frac{\beta s}{2}(\beta-\cos\theta)(2C^1_{22}-2C^1_{23}+C^2_{22}-C^2_{23})+\frac{1}{2}(B^1_0+4C^2_{24}-8C^1_{24}-2D'_{422})\Big\}, \tag{B7}$$

the arguments of the invariant integrals are

$$D'_{i,j,k}=D_{i,j,k}(-k_3,k_1,k_2,M_{H_1},M_\Phi,M_\Phi,M_\Phi)+D_{i,j,k}(-k_3,k_1,k_2,M_{H_2},M_\Phi,M_\Phi,M_\Phi),$$
$$D'_{i,j}=D_{i,j}(-k_3,k_1,k_2,M_{H_1},M_\Phi,M_\Phi,M_\Phi)+D_{i,j}(-k_3,k_1,k_2,M_{H_2},M_\Phi,M_\Phi,M_\Phi),$$
$$C^1_{i,j}=C_{i,j}(k_2,-k_2+k_4,M_\Phi,M_\Phi,M_{H_1})+C_{i,j}(k_2,-k_2+k_4,M_\Phi,M_\Phi,M_{H_2}),$$
$$C^2_{i,j}=C_{i,j}(-k_3,-k_1+k_3,M_\Phi,M_{H_1},M_\Phi)+C_{i,j}(-k_3,-k_1+k_3,M_\Phi,M_{H_2},M_\Phi),$$
$$C^3_{i,j}=C_{i,j}(k_1,-k_1-k_2,M_\Phi,M_\Phi,M_\Phi),$$
$$C^4_{i,j}=C_{i,j}(-k_4,k_3+k_4,M_{H_1},M_\Phi,M_\Phi)+C_{i,j}(-k_4,k_3+k_4,M_{H_2},M_\Phi,M_\Phi),$$
$$B^1_0=B_0(k_1\text{-}k_3,M_\Phi,M_{H_1})+B_0(k_1\text{-}k_3,M_\Phi,M_{H_2}),$$
$$B^2_0=B_0(k_1+k_2,M_\Phi,M_\Phi),$$

where the decomposition of $B$, $C$, and $D$ functions integrals is given in Ref. [11].


[1] L3 Collaboration, Phys. Lett. B **303**, 391 (1993); ALEPH Collaboration, *ibid.* **313**, 299 (1993); DELPHI Collaboration, Nucl. Phys. **B421**, 3 (1994); OPAL Collaboration, Phys. Lett. B **327**, 397 (1994); J. F. Grivaz, presented at the European Physical Society International Europhysics Coference on High Energy Physics, Brussels, Belgium, 1995.

[2] U. Heller, M. Klomfass, H. Neuberger, and P. Vranas, Nucl. Phys. **B405**, 555 (1993); J. Eills, G. L. Fogli, and E. Lisi, Phys. Lett. B **333**, 118 (1994); Z. Phys. C **69**, 627 (1996); K. Hagiwara, S. Matsumoto, D. Haidt, and G. S. Kim, Z. Phys. C **64**, 559 (1994).

[3] J. F. Gunion, H. E. Haber, G. L. Kane, and S. Dawson, *The Higgs Hunter's Guide* (Addison-Wesley, Reading, MA, 1990).

[4] CDF Collaboration, F. Abe *et al.*, Phys. Rev. Lett. **75**, 1017 (1995); D0 Collaboration, S. Abachi *et al.*, *ibid.* **75**, 1034 (1995).

[5] I. F. Ginzburg *et al.*, Nucl. Instrum. Methods Phys. Res. **205**, 47 (1983).

[6] I. F. Ginzburg *et al.*, Nucl. Instrum. Methods Phys. Res. A **219**, 5 (1984).

[7] S. Y. Choi and F. Schrempp, Phys. Lett. B **272**, 149 (1991); G. Belanger and F. Boudjema, *ibid.* **288**, 210 (1992).

[8] A. Denner, S. Dittmaier, and R. Schuster, Nucl. Phys. **B452**, 8 (1995).

[9] A. Denner, Fortschr. Phys. **41**, 307 (1993); K. I. Aoki, Z. Hioki, R. Kawabe, M. Konuma, and T. Muta, Prog. Theor. Phys. **64**, 707 (1980); and **65**, 1001 (1981).
[10] W. Hollik, Z. Phys. C **32**, 291 (1986); **37**, 569 (1988).
[11] G. 't Hooft and M. Veltman, Nucl. Phys. **B153**, 365 (1979); G. Passarino and M. Veltman, *ibid.* **B160**, 151 (1979).
[12] L. Z. Sun, X. X. Chen, W.G. Ma, and Y. Y. Liu, *J. Chin. Univ. Sci. Technol.* **25**(3), 264 (1995).
[13] Pariticle Data Group, R. M. Barnett *et al.*, Phys. Rev. D **54**, 1 (1996); L. Z. Sun and Y. Y. Liu, *ibid.* **53**, 2411 (1996).
[14] H. Veltman, Z. Phys. C **62**, 235 (1994); E. E. Boos and G. V. Jikia, Phys. Lett. B **275**, 164 (1992).